Available on CMS information server

CMS AN -2009/074

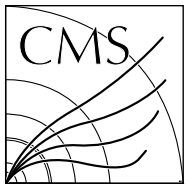

The Compact Muon Solenoid Experiment

Analysis Note

The content of this note is intended for CMS internal use and distribution only

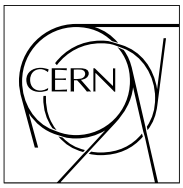

11 May 2009 (v3, 20 May 2009)

Electron Reconstruction at Low $\mathbf{p_T}$

N. Adam, D. Bandurin, D. Ellman, V. Halyo, A. Hunt, J. Werner

Abstract

Accurate and efficient reconstruction of low-p_T electrons is essential for measurement of low mass resonances decaying to di-electrons. Examination of the default GSF electron with Hybrid clustering in the Barrel and Multi5x5 in the Endcap, Particle Flow electron and reevaluation of the GSF electron with Island clustering is described in this note for electrons with Pt less than 10 GeV. Re-tuning the supercluster energy correction for low $E_{\rm T}$ barrel superclusters, reducing minimum supercluster, supercluster seed, and track energies, and opening geometrical matching windows yields a much improved efficiency for low $p_{\rm T}$ electrons.

Contents

1 Introduction

The main focus of electron reconstruction work at CMS has been to optimize the performance of electrons with transverse momenta between 5 and 50 GeV/c [7]. Some attention has also been paid to higher energy electrons, which will be important for the study of high mass resonances [2, 11]. However, for low mass resonances such as $\Upsilon(\mathrm{nS})$ and J/Ψ, the electron transverse momenta peak at a much lower scale than has been considered. For $\Upsilon(1\mathrm{S})$ for example, the peak in electron p_{T} occurs at $\sim$4 GeV/c and a significant fraction ($\sim 40\%$) of the daughter electron has $p_{\mathrm{T}} < 4$ GeV/c. The study of low mass resonances will be important in early data-taking and is motivated on two fronts.

Firstly, the theory of hadroproduction mechanisms for these resonances is not yet understood [6]. A non-relativisitic QCD (NRQCD) factorization is generally used to describe the production of heavy quarkonia states, however, leading-order (LO) prescriptions result in poor descriptions of available data [4]. Better agreement with data can be achieved by adding higher-order and relativistic corrections which favor a color-singlet, over the color-octet model. However neither color singlet or octect model seems to succeed in fully predicting all facets of the production: yield, shape in p_{T}, polarization, etc [4, 9].

A second motivation for studying low mass resonance production with early LHC data is that the masses and widths of such resonances are all well known [1]. This, combined with the fact that $\Upsilon(\mathrm{nS})$ and J/Ψ production cross-sections are large enough to produce significant numbers of events even with accumulated luminosities of only $\sim$ 10 pb^{-1}, enables the use of the resonances as a tool for calibration of electron energy scale at low p_T. The latter, being combined with electron energy scale tuned at Z^0 mass, may give a better extrapolation to higher energies.

The cleanest decay modes for such studies will be leptonic decays, such as $\Upsilon \rightarrow e^+e^-$. It is therefore of vital importance that electron reconstruction be extended to transverse momenta below 5 GeV/c, ideally with some substantial efficiency even for electrons with p_{T} as low as 3 GeV/c. In this note we examine and tune the existing electron reconstruction algorithms and also reevaluate the GSF electron in combination with the Island Algorithm.

2 Overview of Electron Reconstruction (GsfElectrons)

Standard reconstruction of GsfElectrons (electrons formed from tracks made with the Gaussian Sum Filter (Gsf) algorithm) in CMS is described in detail in Ref. [7]. A description of the CMS electromagnetic calorimeter (ECAL) and silicon tracker can be found in Ref. [8]. A basic outline of the electron reconstruction procedure is as follows:

1. **SuperCluster Reconstruction**: Starting from ECAL rec hits use clustering algorithm to reconstruct clusters from electrons and photons. For standard reconstruction the Hybrid SuperCluster algorithm [3] is used in the barrel and the Multi5x5 SuperCluster algorithm is used in the endcaps.
2. **Pixel Matching**: Starting with corrected SuperCluster collections, select silicon tracker (pixel) seeds (sets of two tracker hits) that are matched in η and ϕ to a SuperCluster.
3. **Gsf Track Reconstruction**: Using the pixel seeds from the pixel matching stage (i.e., tracker seeds that have been matched to SuperClusters) form tracks using the Gsf algorithm.
4. **Gsf Electron Reconstruction**: Take the Gsf track collection and their matched SuperClusters and form a "GsfElectron" from each pair. The energy of the final object is taken from either the SuperCluster energy, the track energy or a weighted combination of the two. Which energy is chosen depends on the details of the track and SuperCluster.

At each stage in the electron reconstruction we can make improvements for low p_{T} electrons. In the sections below we will look at each reconstruction stage individually to determine the recommended changes for low p_{T} electrons.

3 Re-tuning GsfElectrons for Low $\mathrm{p_T}$

The various components of the electron reconstruction process are re-tuned here to get the maximum efficiency and best resolution for low p_{T} electrons. In most cases the final outcome will be generally applicable for any low p_{T} electron, however, for the purposes of tuning we concentrate on the case of electrons from $\Upsilon(\mathrm{nS})$ resonances.

In many ways $\Upsilon(\mathrm{nS})$'s provide the ideal case on which to tune. The daughter electrons are very low p_{T} and the production cross-sections are not large enough that we can afford to throw away the lowest p_{T} electron daughters and keep only the high p_{T} tail, such as may be done in the case of J/Ψ. We concentrate on keeping electrons with $p_{\mathrm{T}} > 3$ GeV/c, since this will likely be the lower limit for any possible triggers [5].

3.1 SuperCluster Algorithms

Once the electron deposits energy in the ECAL, this energy is generally spread over several ECAL crystals in close geometrical proximity. These crystals are treated as a single object, called a cluster. The energy deposited per crystal in a cluster tends to be at a maximum for a central cell and decrease towards the edges of the cluster. However, the cluster geometry is complicated by the electron radiation its interaction with detector material and the ECAL noise. Since electrons follow a helical trajectory in the detector's magnetic field, they tend to radiate bremsstrahlung photons that are relatively localized in η but spread in ϕ. Each photon above the critical energy can form its own ECAL cluster. Sometimes these photons interact with the detector material and produce an e^+e^- pair. These pair produced electrons may or may not reach the ECAL depending on where they were produced and their p_T, and their probablity to radiate photons. In order to account for as much of the initial electron energy as possible, the energy deposits of the initial electron, radiated photons, and pair produced electrons are combined into a cluster of clusters, called a supercluster. The goal in forming superclusters is to do so in a manner that distinguishes small energy deposits from detector noise. There are various algorithms for creating superclusters. At CMS the default algorithms are the Hybrid clustering algorithm in the barrel, and the Multi5x5 clustering algorithm in the endcaps. In the barrel, for low p_{T} electrons, we would first study the performance of the Hybrid clustering algoritm and re-examine the possibility of using an Island clustering algorithm.

3.1.1 Hybrid Barrel SuperClusters

The Hybrid algorithm [3] starts from a seed crystal (ECAL rec hit) that represents a local energy maximum in the calorimeter and passes a minimum energy threshold, $E_{\mathrm{T}}^{\mathrm{hybseed}}$. A "domino" of crystals is formed around seed crystal, it is centered on the seed and extended in η. The domino may be either 1×3 crystals or, if the seed energy is greater than E_{wing}, 1×5 crystals. Adjacent dominoes are added to the supercluster in each direction in ϕ until N_{step} dominoes are added in each direction. Dominoes with energy below E_{thresh} are removed in order to account for detector noise. The dominoes of the supercluster are then broken into basic clusters in ϕ, with each basic cluster requiring a seed domino with energy greater than E_{seed}. Each threshold and/or search range used in the algorithm has default values that are optimal for finding electrons with $p_{\mathrm{T}} > 5$ GeV/c. All these parameters can be adjusted to provide greater efficiency for low p_{T} electrons. The CMS default values are shown in Table 1.

Parameter	Default Value	Steps for Tuning					Re-tuned Value
$E_{\mathrm{T}}^{\mathrm{hybseed}}$ (GeV)	1.0	0.2	0.4	0.6	0.8	1.0	0.6
N_{step}	17	17	21	23			23
E_{wing} (GeV)	0.0			-			0.0
E_{thresh} (GeV)	0.1			-			0.1
E_{seed} (GeV)	0.35			-			0.35

Table 1: Table of parameters for the Hybrid algorithm. Here $E_{\mathrm{T}}^{\mathrm{hybseed}}$ gives the minimum E_{T} for a hybrid supercluster seed crystal, N_{step} gives the number of crystals to search in ϕ (in each direction), E_{wing} gives the threshold for using 1×5 crystals, E_{thresh} gives the threshold for using a domino, and E_{seed} gives the minimum domino energy to make a disconnected basic cluster. The tuning steps show the alternative thresholds considered for each parameter for low p_{T} tuning. Final values are chosen using maximum $\Upsilon(\mathrm{nS})$ signal significance from the final electron reconstruction (see Section 3.6).

3.1.2 Island Barrel SuperClusters

In the Island algorithm the reverse approach to supercluster building is taken. First disconnected basic clusters are found, then these are joined to create Island superclusters [3]. To create basic clusters the Island algorithm searches for crystals with transverse energy above a certain threshold, $E_{\mathrm{T}}^{\mathrm{seed}}$. A seed is removed from the list if it is adjacent to a higher energy seed. The algorithm then clusters crystals belonging to each seed by searching in ϕ and η until a

rise in energy, or a "hole" (zero-suppressed crystal) is found. These form the "basic" clusters. Searching in fixed ϕ and η windows around the most energetic clusters (above some threshold, $E_{\rm T}^{\rm islseed}$), basic clusters can be collected to form the Island superclusters. Parameters for the Island algorithm are shown in Table 2.

Parameter	Default Value	Steps for Tuning					Re-tuned Value
$E_{\rm T}^{\rm seed}$ (GeV)	0.5	0.1	0.2	0.3	0.4	0.5	0.3
$E_{\rm T}^{\rm islseed}$ (GeV)	1.0	0.2	0.4	0.6	0.8	1.0	0.6
$\Delta\phi_{\rm island}$	0.8	0.8	1.0	1.2			1.2
$\Delta\eta_{\rm island}$	0.06			-			0.06

Table 2: Table of parameters for the Island algorithm. Here $E_{\rm T}^{\rm seed}$ gives the minimum $E_{\rm T}$ for an island basic cluster seed crystal, $E_{\rm T}^{\rm islseed}$ gives the minimum E_T for a basic cluster to seed a supercluster, $\Delta\phi_{\rm island}$ gives the search window in ϕ used to look for basic cluster components of a supercluster, and $\Delta\eta_{\rm island}$ gives the search window in η used to look for basic cluster components of a supercluster. The tuning steps show the alternative thresholds considered for each parameter for low $p_{\rm T}$ tuning. Final values are chosen using maximum $\Upsilon({\rm nS})$ signal significance from the final electron reconstruction (see Section 3.6). The first two parameters, $E_{\rm T}^{\rm seed}$ and $E_{\rm T}^{\rm islseed}$, are tuned together, i.e., the crystal seed threshold is always half of the basic cluster seed threshold.

3.1.3 Multi5x5 Endcap SuperClusters

The ECAL endcap uses the Multi5×5 superclustering algorithm. The basic strategy for this algorithm is to construct fixed-size basic clusters of 5×5 crystals and then combine the basic clusters into supercluster objects. The algorithm starts with all the endcap crystal hits that are local maxima and above tranverse energy threshold $E_{\rm T}^{\rm seed}$. Starting with the highest energy crystal seed, a 5×5 crystal cluster is made around the seed. Once a crystal is assigned to one cluster it is not available to be added to other clusters, but crystals on the edge of a cluster are still allowed to seed other clusters.

Once all the basic clusters are made, the superclustering process combines basic clusters. The superclustering algorithm is a bremsstrahlung recovery process which, like the Island algorithm, seeks to account for clusters that are relatively spread in ϕ but localized in η. This process starts with a list of basic cluster "seeds", that is basic clusters that have a transverse energy of at least $E_{\rm T}^{\rm multiseed}$. In order of energy, all other basic clusters have a chance to be added to the seed cluster's supercluster. A basic cluster is added if it has η and ϕ positions that are within the η and ϕ roads of the seed cluster. The η and ϕ roads are defined by the parameters $\Delta\eta_{\rm multi}$ and $\Delta\phi_{\rm multi}$, which are the absolute values of the largest allowed seed cluster-to-other cluster distances. After all basic clusters are matched to the seed cluster, if the highest energy unmatched cluster has enough energy to seed a supercluster another matching process begins. Superclusters which are formed in the ECAL endcaps are later combined with energy deposits in the preshower detectors which are directly in front of the endcaps. The parameters for the Multi5×5 superclustering algorithm are listed in table 3.

Parameter	Default Value	Steps for Tuning					Re-tuned Value
$E_{\rm T}^{\rm seed}$ (GeV)	0.18			-			0.18
$E_{\rm T}^{\rm multiseed}$ (GeV)	1.0	0.2	0.4	0.6	0.8	1.0	0.6
$\Delta\phi_{\rm multi}$	0.6	0.6	0.7	0.8			0.8
$\Delta\eta_{\rm multi}$	0.06			-			0.14

Table 3: Table of parameters for the Multi5×5 algorithm. Here $E_{\rm T}^{\rm seed}$ gives the minimum $E_{\rm T}$ for a multi5×5 basic cluster seed crystal, $E_{\rm T}^{\rm multiseed}$ gives the minimum E_T for a basic cluster to seed a supercluster, $\Delta\phi_{\rm multi}$ gives the search window in ϕ used to look for basic cluster components of a supercluster, and $\Delta\eta_{\rm multi}$ gives the search window in η used to look for basic cluster components of a supercluster. The tuning steps show the alternative thresholds considered for each parameter for low $p_{\rm T}$ tuning. Final values are chosen using maximum $\Upsilon({\rm nS})$ signal significance from the final electron reconstruction (see Section 3.6).

3.2 SuperCluster Energy Corrections

After the clustering algorithms, the raw supercluster energy needs to be corrected to account for the angle at which the particles have entered the ECAL, as well as energy loss from bremstraalung and energy spread. Corrections are applied differently for the Hybrid and Multi5x5 algorithms as compared to the Island algorithm.

3.2.1 Hybrid and Multi5x5 Corrections

For these algorithms the energy correction is applied in three stages to account for each of the effects mentioned aboved. **The first correction,** $f(E,\eta)$, corrects for shower leakage due to the jagged ECAL surface from the projection of the ECAL barrel crystals. This correction is not applied to the endcap region, where the crystal geometry reduces shower leakage.

$$f(E,\eta) = \begin{cases} E & |i_\eta| < p_0 \\ E/(1+p_1(|i_\eta|-p_0)^2) & |i_\eta| \geq p_0 \end{cases},$$

where $|i_\eta| = |\eta| \times (5/0.087)$.

The second correction, $f(E,\sigma_\phi/\sigma_\eta)$, takes into account the relative energy spread in the ϕ and η direction, where σ_ϕ and σ_η are the supercluster ϕ and η widths respectively. These are defined as $\sqrt{\sum_i (E_{cry_i}\Delta x_i^2)/E_{SC}}$, where Δx is the difference between the i^{th} crystal and the supercluster center in ϕ or η. This correction is applied in both the ECAL barrel and endcap regions. In the barrel it is applied to the corrected energy after $f(E,\eta)$, while in the endcap it is applied to the raw supercluster energy.

$$f(E,\sigma_\phi/\sigma_\eta) = \begin{cases} E/(p_{4,24}d^2 + p_{5,25}d + p_{6,26}) & d < p_{8,28} \\ E/(ad^2+bd+c) & d \geq p_{8,28} \end{cases}$$

$$\begin{aligned} a &= p_{7,27} \\ b &= 2p_{8,28}(p_{4,24} - p_{7,27}) + p_{5,25} \\ c &= p_{4,24}p_{8,28}^2 + p_{5,25}p_{8,28} + p_{6,26} - p_{7,27}p_{8,28}^2 - bp_{8,28} \end{aligned}$$

$$d = \begin{cases} \sigma_\phi/\sigma_\eta & p_{2,22} \leq \sigma_\phi/\sigma_\eta \leq p_{3,23} \\ p_{2,22} & \sigma_\phi/\sigma_\eta \leq p_{2,22} \\ p_{3,23} & \sigma_\phi/\sigma_\eta \geq p_{3,23} \end{cases}$$

where $p_2, \ldots, p_8$ are for barrel corrections and $p_{22}, \ldots, p_{28}$ are for endcap corrections.

The third correction, $f(E_T,\eta)$ is a transverse energy correction applied to both the barrel and endcap regions. It is applied to the transverse component of the corrected energy from $f(E,\sigma_\phi/\sigma_\eta)$, where $E_T \equiv E/\cosh(\eta) \equiv E\sin(\theta)$.

$$f(E_T,\eta) = E_T/\alpha$$

$$\alpha = \begin{cases} a & a \geq 0.5 \\ 0.5 & a < 0.5 \end{cases}$$

$$\begin{aligned} a_{barrel} &= b_{barrel} + c_{barrel}\arctan(p_{17}(p_{18} - |\eta|) + p_{19}|\eta|) \\ b_{barrel} &= p_9 + p_{10}/(E_T + p_{11}) + p_{12}/E_T^2 \\ c_{barrel} &= p_{13} + p_{14}/(E_T + p_{15}) + p_{16}/E_T^2 \end{aligned}$$

$$\begin{aligned} a_{endcap} &= b_{endcap} + c_{endcap}|\eta| + d_{endcap}\eta^2 \\ b_{endcap} &= p_{29} + p_{30}/E_T \\ c_{endcap} &= p_{31} + p_{32}/E_T \\ d_{endcap} &= p_{33} + p_{34}/E_T \end{aligned}$$

The default supercluster energy correction is very poor for low E_T hybrid superclusters, over-correcting in the outer barrel, and under-correcting in the central barrel. The corrections were re-tuned on low p_{T} electrons gun MC. Table 4 lists the default and re-tuned energy correction parameters. Retuned parameters are only shown

where changes were made. Figure 1 shows the improvement in the ratio of supercluster E_T to generated electron E_T for default and new corrections for barrel electrons with p_T between 3 and 6 GeV/c, where the new correction is designed to perform best. Figure 2 shows the data that was fit to get the re-tuned energy correction ($f(E_T, \eta)$ in the barrel) and shows the performance of the correction.

$f(E, \eta)$, barrel			$f(E, \eta)$, endcap		
Parameter label	default value	retuned value	Parameter label	default value	retuned value
p_0	40.2198		NA	NA	NA
p_1	-3.03103$\times 10^{-6}$				
$f(E, \sigma_\phi/\sigma_\eta)$, barrel			$f(E, \sigma_\phi/\sigma_\eta)$, endcap		
Parameter label	default value	retuned value	Parameter label	default value	retuned value
p_2	1.1		p_{22}	0.6	
p_3	8.0		p_{23}	6.0	
p_4	-0.05208		p_{24}	-0.04163	
p_5	0.1331		p_{25}	0.08552	
p_6	0.9196		p_{26}	0.95048	
p_7	-0.0005735		p_{27}	-0.002308	
p_8	1.343		p_{28}	1.077	
$f(E_T, \eta)$, barrel			$f(E_T, \eta)$, endcap		
Parameter label	default value	retuned value	Parameter label	default value	retuned value
p_9	1.0012	1.41059	p_{29}	0.9746	
p_{10}	-0.5714	-2.86873	p_{30}	-6.512	
p_{11}	0		p_{31}	0.02771	
p_{12}	0		p_{32}	4.983	
p_{13}	0		p_{33}	-0.007288	
p_{14}	0.5549	-0.664671	p_{34}	-0.9446	
p_{15}	12.74	44.8328			
p_{16}	1.0448	2.8634			
p_{17}	8.0	4.0883			
p_{18}	1.023	1.47804			
p_{19}	-0.00181	-0.0092684			

Table 4: Default and retuned parameters for supercluster energy corrections.

Since the new energy correction is tuned for low p_T electrons, it does not perform well in the higher $p_{\rm T}$ regions. Therefore the re-tuned supercluster energy correction is used for superclusters with raw energy less than 5 GeV, while the default parameters are applied for higher energies. Figure 3 shows why the cutoff value of 5 GeV was chosen based on the ratio of $E_{\rm T}$ of matched superclusters to the $E_{\rm T}$ of generated electrons.

Imposing an energy cut-off for the correction, however, is problematic: because a given raw supercluster energy can represent a large range of true electron energies, hence a discontinuity in the resolution results at the cut-off value. Figure 4 shows this effect in terms of efficiency. Figure 5 shows the supercluster energy resolution using the retuned reconstruction.

3.2.2 Island Corrections

The default Island supercluster energy correction is a parametric function of the number of crystals in the seed basic cluster of the supercluster. This correction is supposed to account for all the effects discussed above. However,

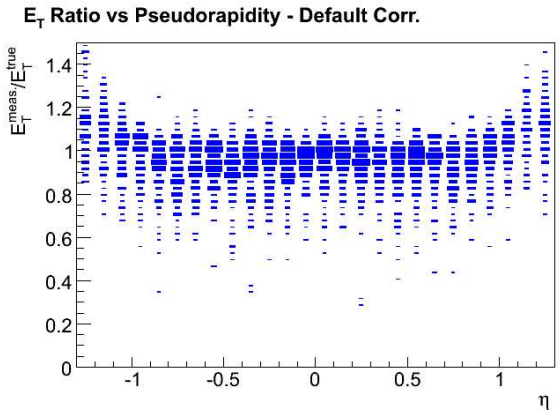

(a) Default Correction

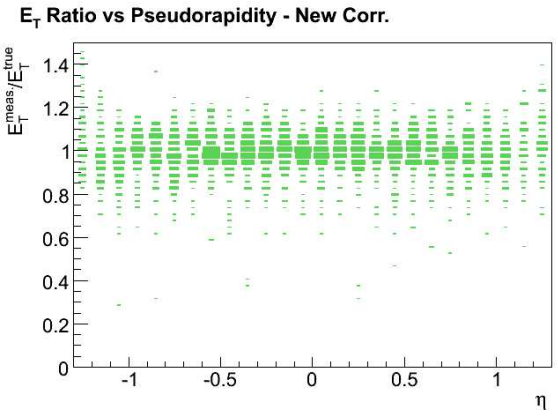

(b) New Correction

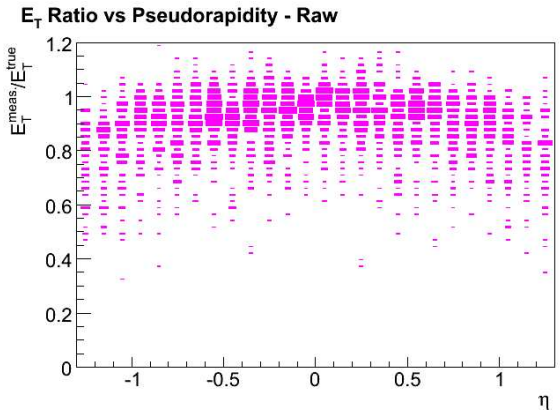

(c) Raw Supercluster

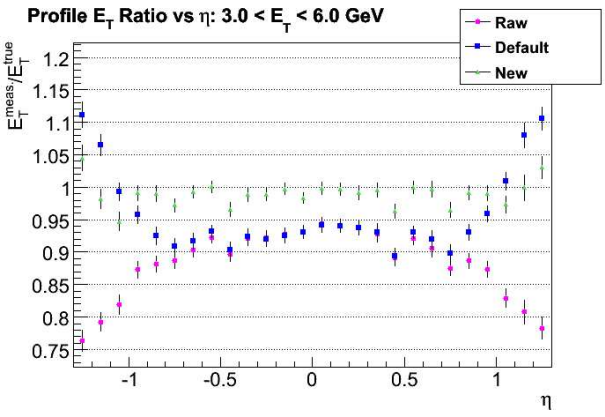

(d) Profile of 1(a), 1(b), and 1(c).

Figure 1: Ratio of supercluster E_T to generated electron E_T against psuedorapidity for barrel electrons with p_T between 3 and 6 GeV/c.

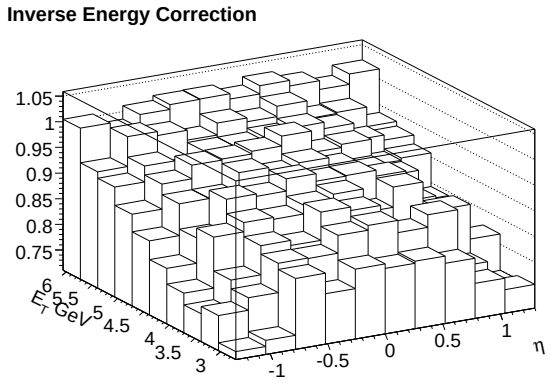

(a) Inverse $f(E_T, \eta)$

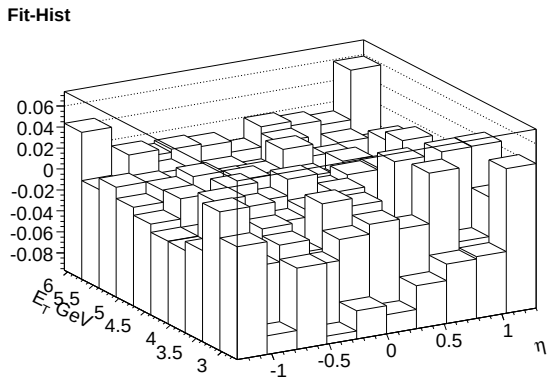

(b) Fit $E_{\mathrm{T,meas.}}/E_{\mathrm{T,true}}$ - True $E_{\mathrm{T,meas.}}/E_{\mathrm{T,true}}$

Figure 2: 2(a): The inverse of the retuned $f(E_T, \eta)$ barrel supercluster energy correction (i.e. the data that was fit to get the correction); 2(b): The difference between the corrected E_T and true E_T.

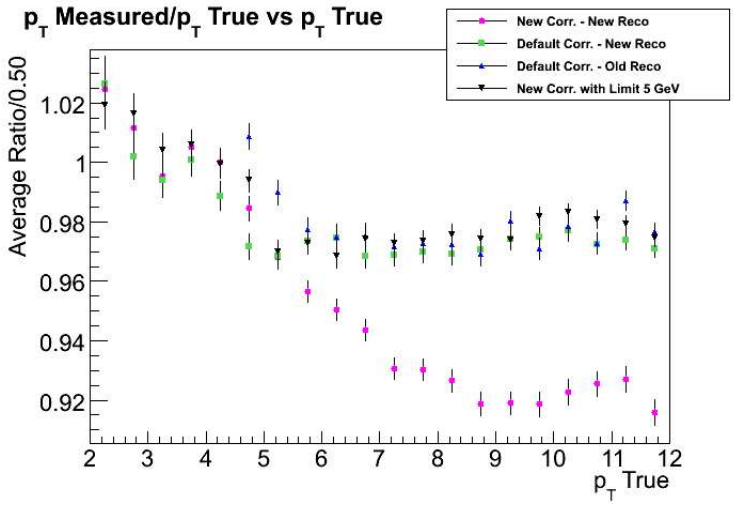

Figure 3: Average p_T ratio of reconstructed to generated electrons for various reconstruction and energy correction combinations. The default energy correction performs better than the new correction for electrons with p_T above 5 GeV/c.

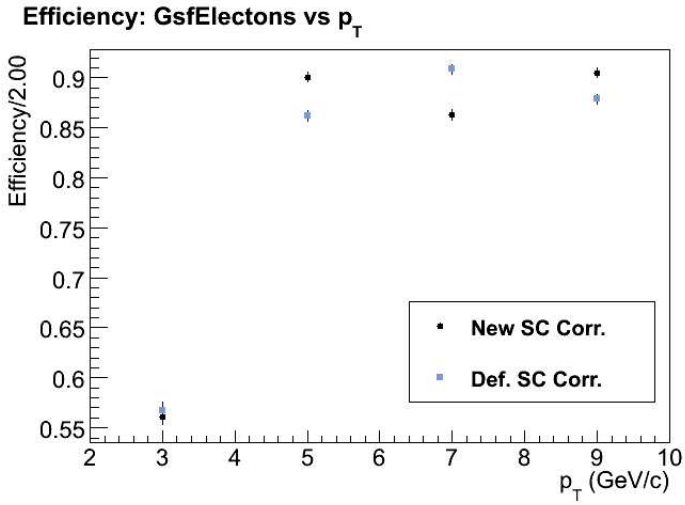

Figure 4: Efficiency vs p_T for electrons with the new and default supercluster energy corrections.

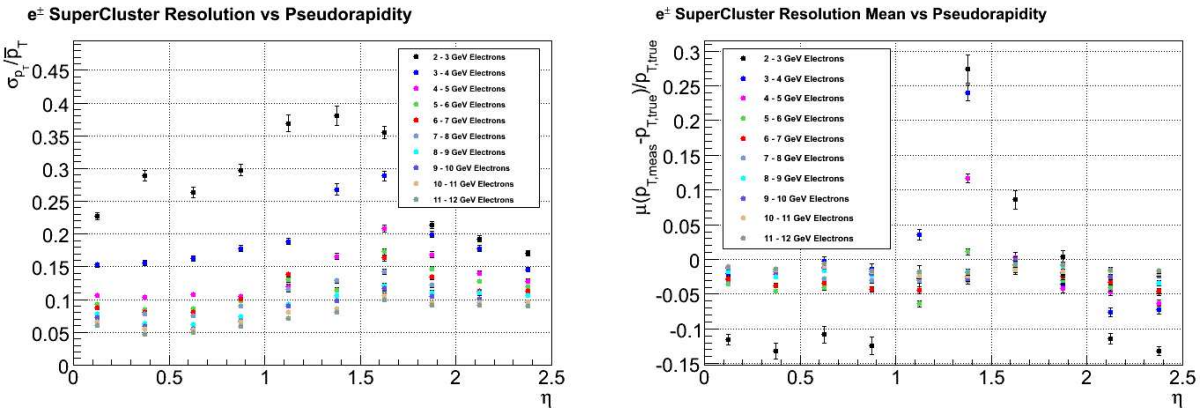

Figure 5: Supercluster energy resolution.

Parameter	Value from Fit
p_1	0.015 ± 0.001
p_2	-0.99 ± 0.01
p_3	0.088 ± 0.009
p_4	1.37 ± 0.05
p_5	-0.013 ± 0.004
p_6	0.27 ± 0.03

Table 5: Parameter values from a fit to the inverse energy correction for the island supercluster energies.

this simple function fails to fully correct the supercluster energy in the $E_{\rm T}$ range we are concerned with. Looking at the two-dimensional distribution of average measured-to-true supercluster $E_{\rm T}$ ratios versus supercluster $E_{\rm T}$ and η, Figure 6(a), it is obvious that an additional correction is required. This correction must be a function of $E_{\rm T}$ and η just as in the case of the Hybrid and Multi5x5 algorithms. In fact this histogram effectively gives the inverse of the required energy correction. We fit this histogram with a function, $f(E_{\rm T}, \eta)$, that represents the general form of the inverse energy correction. The η dependence of the inverse correction has linear and $\arctan$ components. The $E_{\rm T}$ dependence enters linearly into the parameters of these functions, so that we may write the general form of the island correction as:

$$f(E_{\rm T}, \eta) = (p_1 E_{\rm T} + p_2)(\arctan\left(-1.0((p_3 E_{\rm T} + p_4) - |\eta|)\right) + (p_4 E_{\rm T} + p_5)|\eta|, \quad (1)$$

where the p_n are free parameters. Fitting with this form we find the parameter values as given in Table 5. The goodness of the fit (correct to within 2%) is shown in Figure 6(b). In addition we make some small adjustments to flatten out the η distribution, as well as an overall scale adjustement. The final correction, $F_{\rm island}$, is given by:

$$F_{\rm island} = \begin{cases} 0.97/(0.98888 f(E_{\rm T}, \eta)), & |\eta| < 0.05 \\ 0.97/(-0.072|\eta| + 1.0072) f(E_{\rm T}, \eta)), & 0.05 < |\eta| < 0.5 \\ 0.97/f(E_{\rm T}, \eta), & |\eta| > 0.5 \end{cases} \quad (2)$$

The supercluster energy ratio (measured to true) is shown in Figure 7 for raw energy, default corrected energy and the new corrected energy from Eq. 2.

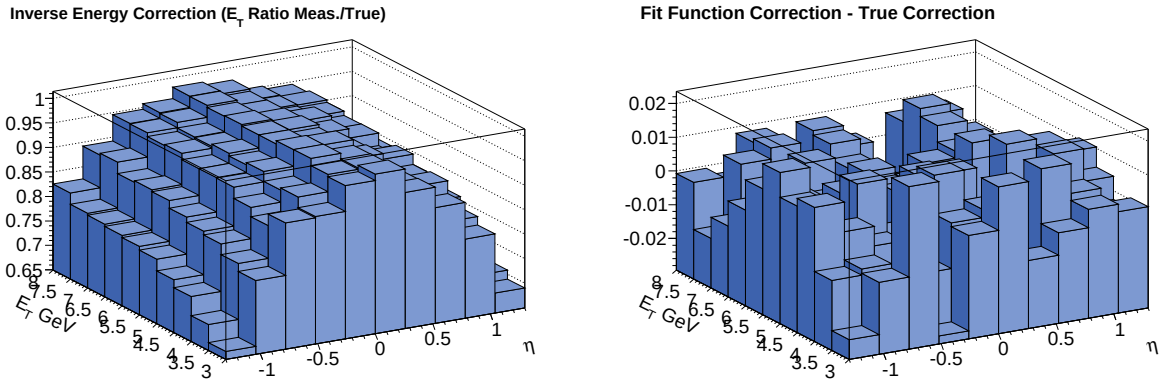

(a) Inverse $f(E_T, \eta)$

(b) Fit $E_{\rm T,meas.}/E_{\rm T,true}$ - True $E_{\rm T,meas.}/E_{\rm T,true}$

Figure 6: Correction in η and $E_{\rm T}$ to Island supercluster energies. Figure 6(a) shows the average ratio of measured to true supercluster $E_{\rm T}$ versus supercluster $E_{\rm T}$ and η. It effectively give the inverse energy correction. Figure 6(b) shows the results of the 2D fit in $E_{\rm T}$ and η, $f(E_T, \eta)$, to the inverse energy correction. The results are shown as $f(E_{\rm T}, \eta)$ - $H(E_{\rm T}, \eta)$, where $H(E_{\rm T}, \eta)$ gives the true correction from MC.

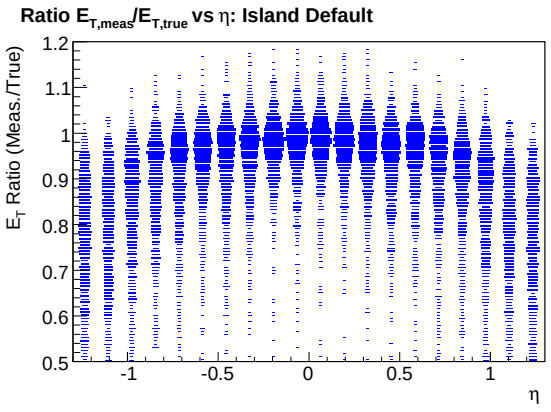

(a) Default Correction

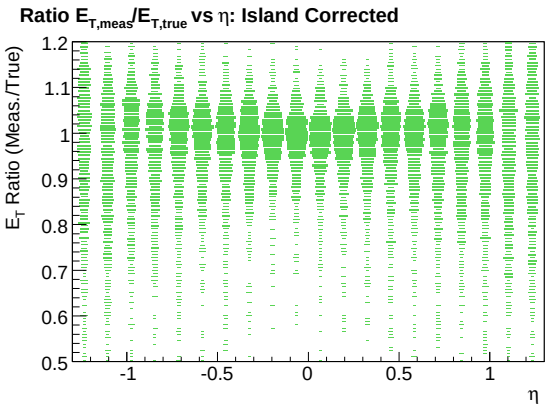

(b) New Correction

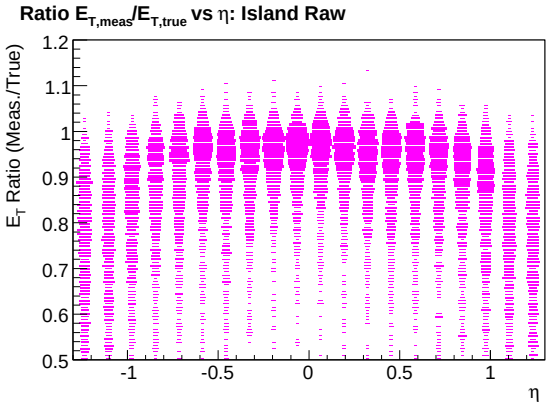

(c) Raw Supercluster

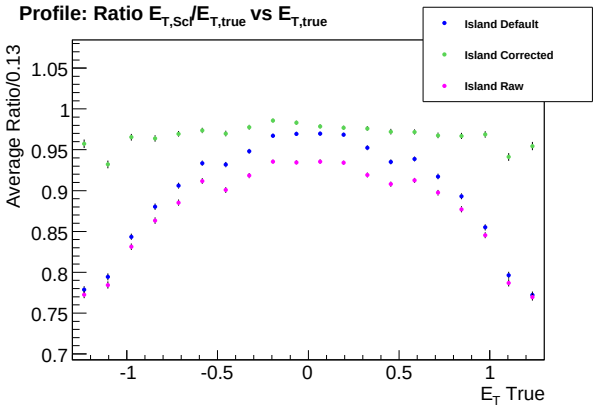

(d) Profile of 1(a), 1(b), and 1(c).

Figure 7: Ratio of Island supercluster E_{T} to generated electron E_{T} against psuedorapidity for barrel electrons with p_{T} between 3 and 12 GeV/c.

3.3 Pixel Matching

The reconstruction of an electron track starts with hits in the pixel tracker known as a track seed. An electron track seed must be compatible with an ECAL supercluster. The supercluster used to create an electron candidate would have to have corrected E_T of at least E_T^{min} and all of its basic clusters that make up the supercluster would have H/E less than H/E^{max}. Table 6 lists default values and retuned values where they were changed.

Table 6: Default and retuned cuts for using a supercluster

Parameter description	label	default value	retuned value
Minimum E_T for using a supercluster	E_T^{min}	4 GeV	2 GeV
Maximum ratio of HCAL to ECAL E in a basic cluster	H/E^{max}	0.1	

In order to match a track seed to an eligiable supercluster, tracks are constructed from the center of the supercluster to the beam interaction point for both charge hypothesis assuming the supercluster energy. If the supercluster correctly measures the electron energy, this track should be close to the track of a non-radiating electron in the detector's magnetic field. Matching is then done between this supercluster-based track and pixel hits, since there is little time for the electron to deviate from the non-radiating path between the interaction point and the pixel detector. We require two pixel hits to match windows in ϕ and z. The first pixel hit is looked for in the innermost layer of the pixel tracker, or if no match is found, in the next-to-innermost layer. If a first pixel hit is found, a new track is reconstructed using information form the supercluster and the first hit. The second pixel hit must match this new track and is searched for in the next pixel layers. For the first pixel hit, the Δz window depends on the z-width of the beam spot ($\sigma_z^{beamspot}$) and its error (ϵ_{σ_z}) while the $\Delta\phi$ window is dynamically set depending on the supercluster's E_T. The algorithm for determining the widths of the first Δz and $\Delta\phi$ windows ($\sigma_{\Delta z}$ and $\sigma_{\Delta\phi}$) is given below. For the second pixel hit, both windows are fixed and are centered on the expected values of z and ϕ.

$$\sigma_{\Delta z} = \Delta z^{high} - \Delta z^{low}$$

$$\Delta z^{high} = z_{beamspot} + 3\sqrt{\left(\sigma_z^{beamspot}\right)^2 + \left(\epsilon_{\sigma_z}\right)^2}$$
$$\Delta z^{low} = z_{beamspot} - 3\sqrt{\left(\sigma_z^{beamspot}\right)^2 + \left(\epsilon_{\sigma_z}\right)^2}$$

$$\sigma_{\Delta\phi} = \begin{cases} a/E_T + c & E_T^{low} \le E_T \le E_T^{high} \\ a/E_T^{low} + c & E_T < E_T^{low} \\ a/E_T^{high} + c & E_T > E_T^{high} \end{cases}$$

$$\begin{aligned} \Delta\phi_{e^+}^{high} &= \alpha\sigma_{\Delta\phi} \\ \Delta\phi_{e^+}^{low} &= -(1-\alpha)\sigma_{\Delta\phi} \\ \Delta\phi_{e^-}^{high} &= (1-\alpha)\sigma_{\Delta\phi} \\ \Delta\phi_{e^+}^{low} &= -\alpha\sigma_{\Delta\phi} \end{aligned}$$

For our relatively low-p_T analysis, the default pixel matching windows were too narrow. Table 7 gives the default and retuned parameters for determining pixel matching windows.

Figure 8 gives a sense of the $\sigma_{\Delta\phi}$ distribution between extrapolated supercluster position and track position at vertex by using the $\Delta\phi$ distribution between reconstructed supercluster position in the ECAL and GSF track position at vertex for superclusters and tracks that were matched to generated electrons. While using the supercluster position in the ECAL rather than an extrapolated position at the vertex will give incorrect $\Delta\phi$ values, the width of the $\Delta\phi$ distribution is relatively accurate. (Since the change in ϕ from the extrapolation procedure depends on the supercluster E_T and distance from the beam axis, the $\Delta\phi$ vs E_T distribution in the barrel, which has uniform distance from the beam axis, will be shifted but have approximately the same width.) While our first dynamic ϕ window for pixel to supercluster matching depends only on supercluster E_T, we see that there is a strong dependence on η in the endcap region. In the future, a dynamic ϕ window that depends on η could yield improved results.

Table 7: Default and retuned parameters for track seed pixel matching

Parameter	default value	retuned value
a	0.875	1.70
c	0.055	0.1
E_T^{low}	5 GeV	1 GeV
E_T^{high}	35 GeV	
α	0.65	
$\Delta\phi$-2^{nd} pixel hit	0.04	0.12
Δz-2^{nd} pixel hit	0.18 cm	

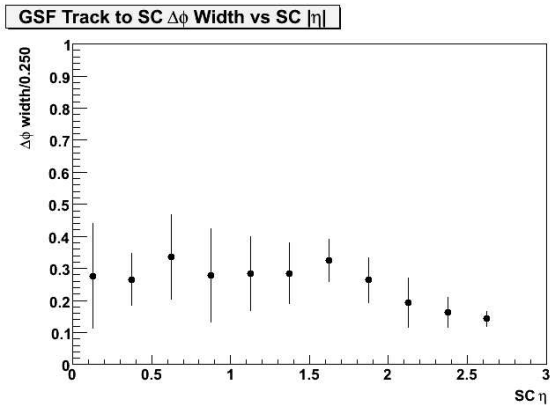

(a) Versus SC η

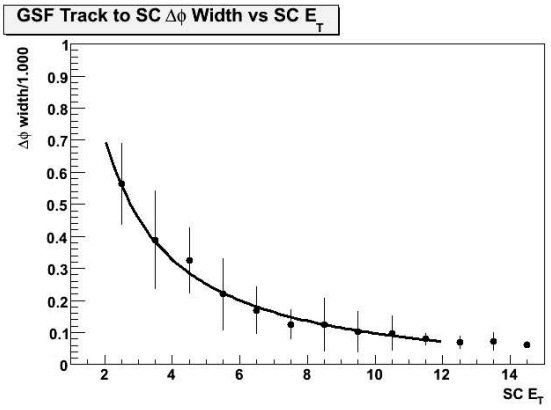

(b) Versus SC p_T, all

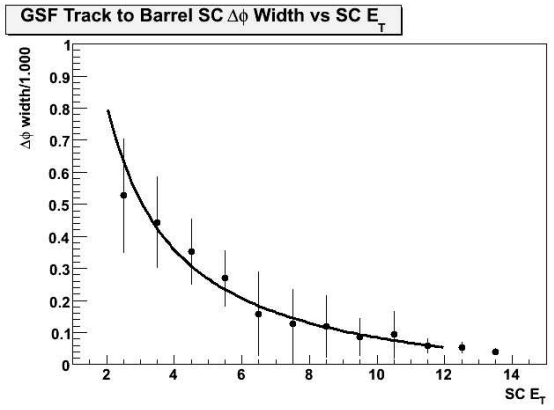

(c) Versus SC p_T, barrel

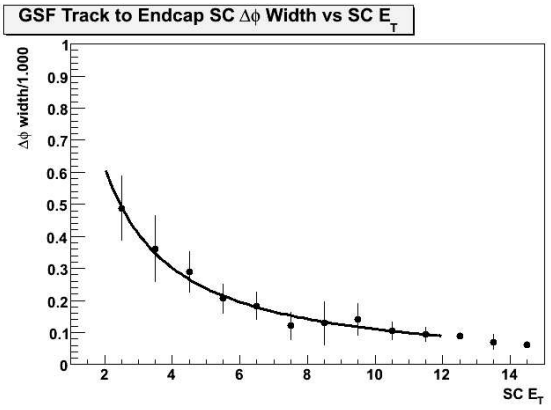

(d) Versus SC p_T, endcap

Figure 8: $\Delta\phi$ width ($\sigma_{\Delta\phi}$) versus supercluster η and E_T for an electron gun with electron p_T between 2 and 12 GeV/c. $\sigma_{\Delta\phi}$ is defined on these graphs as the width of the supercluster to GSF track $\Delta\phi$ window which contains 95% of the events in each η or E_T bin. The error is how much wider the window would have to be to contain 97.5% of events. Fits on the width versus E_T graphs were $a/E_T + c$ with values: 8(b): $a = 1.5 \pm 0.3, c$ insignificant; 8(c): $a = 1.8 \pm 0.4, c$ insignificant ; 8(d): $a = 1.3 \pm 0.2, c$ insignificant.

Figure 9 shows the improvement in GSF track efficiency with the new ϕ matching. The improvement is most dramatic in the outer barrel region, where the large amount of tracker material causes great fluctuations in low-p_T electron tracks.

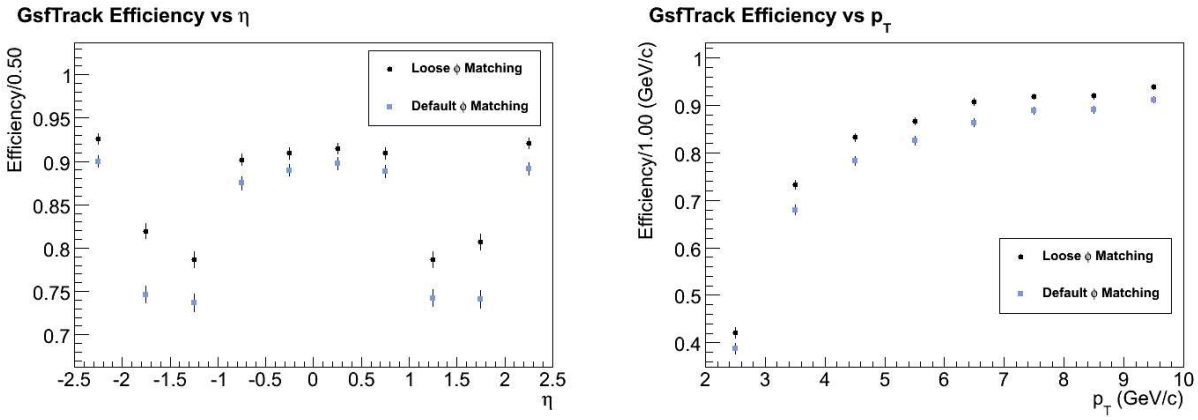

(a) Versus η

(b) Versus p_T

Figure 9: GSF track efficiency vs η and p_T for default and new supercluster to pixel ϕ windows.

3.4 Gsf Fit Tracks

A track trajectory is built using seeds that survive the pixel matching. Matching tracker hits are searched for on the next tracker layers and then an extrapolation of the trajectory is performed using a Bethe-Heitler modeling of the electron losses and a Gaussian Sum Filter (GSF) [7]. The Bethe-Hitler model predicts the probability density function (PDF), $f(z)$, of an electron's energy loss is

$$f(z) = \frac{[-\ln z]^{c-1}}{\Gamma(c)}, c = t/\ln 2,$$

where t is the path length in the material in radiation length and z is the fraction of the energy remaining after the material is traversed [10]. The GSF approximates the bremsstrahlung energy loss of electrons PDF with a mixture of Gaussians rather than a single Gaussian. This procedure repeats until the outer tracker layer, unless no hit is found in two consecutive tracker layers. At each stage the three tracks with the best χ^2 are kept while other possible tracks are discarded. A minimum of five hits ($N_{minhits}$) is required to create a track. Default GSF tracks must have at minimum p_T (p_T^{min}) of 3 GeV, but we lowered the default value to 1 GeV. Tracks then undergo a trajectory smoothing, where the GSF is applied to the track hits in order to estimate the track parameters at each tracker layer. Table 8 gives some parameters for GSF track building.

Table 8: Default and retuned parameters for GSF track building

Parameter	default value	retuned value
$N_{minhits}$	5	
p_T^{min}	3 GeV/c	1 GeV/c

Figure 10 shows the GSF track energy resolution using the retuned reconstruction compared to Kalman tracks.

3.5 Gsf Electrons

If a supercluster and a GSF track are created, a final selection determines if the supercluster and the track are compatible and can thus create an electron candidate. There is a geometrical matching in ϕ and η between the

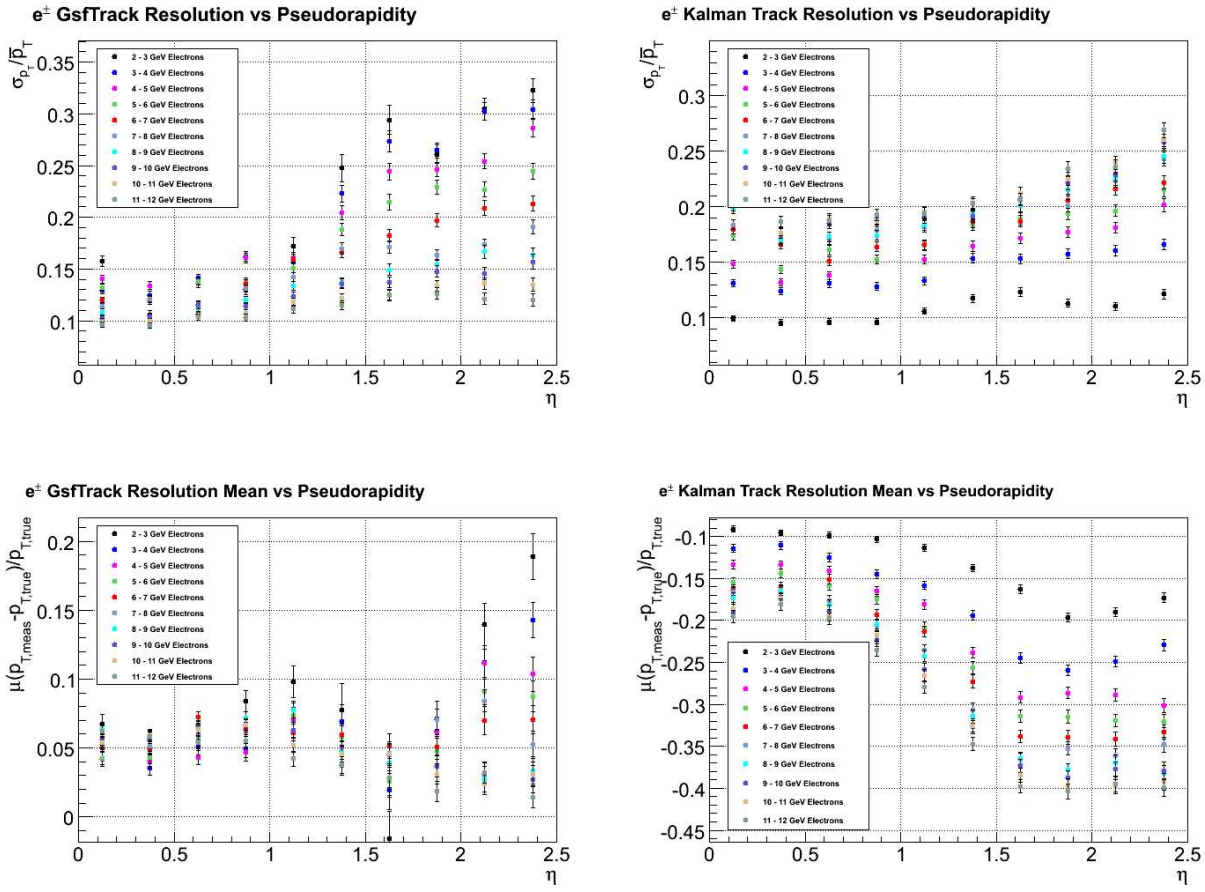

Figure 10: GSF track and Kalman track energy resolution

energy-weighted supercluster position (ϕ_{sc} and η_{sc}) and the extrapolated position of the track at the ECAL using the track parameters at vertex and assuming the trajectory is a perfect helix (ϕ_{in}^{extrap} and η_{in}^{extrap}) [7]. Table 9 lists the default and retuned cuts for creating an electron candidate.

Table 9: Default and retuned cuts for GSF track-supercluster matching

Parameter	default max	retuned max
$\lvert\Delta\phi_{in}\rvert = \lvert\phi_{sc} - \phi_{in}^{extrap}\rvert$	0.1	0.25
$\lvert\Delta\eta_{in}\rvert = \lvert\eta_{sc} - \eta_{in}^{extrap}\rvert$	0.02	0.06

If a supercluster and a track are compatible, their energy values are combined to give a final electron momentum. The weighted mean of the corrected super cluster energy (E_{corr}) and the track momentum at vertex (p) is used when $|E_{corr}/p - 1| < 2\sigma_{E/p}$, with weights defined as the normalized inverse variance of each measurement and where $\sigma_{E/p}$ is the quadratic sum of E_{corr} and p uncertainties. If $|E_{corr}/p - 1| > 2\sigma_{E/p}$, then the electron energy is chosen to be either E_{corr} or p, depending on the electron candidate parameters. In general, low-p_T electrons use the track momentum and high-p_T electrons use the supercluster energy when the values differ sufficiently.

3.6 Significance Tuning

Figures 11 and 12 show the plots that were used to decide the values of $E_T^{hybseed}$ and E_T^{min}, the minimum supercluster seed transverse energy and the minimum total supercluster transverse energy. Data is shown with and without an opened ϕ pixel matching window (described below),and with and without a double 3 GeV electron HLT. Tuning is done to maximize significance ($S/\sqrt{S+B}$, where S is number of signal events and B is number of background events) and efficiency. Since it is difficult to distinguish the significance of the cuts with the HLT within statistical error, we look to the data without the HLT for help. Our chosen cuts of $E_T^{hybseed} = 0.6GeV$ and $E_T^{min} = 2GeV$ provide the best significance with loose and default ϕ windows when there is no HLT and are within the statistical error of the best cuts for data with the HLT. Also, while $E_T^{min} = 3GeV$ has close to the same significance, a cut of $E_T^{min} = 2GeV$ gives a greater signal efficiency. Figures 13, 14, and 15 give significance for these cuts for Υ with daughters split into barrel/barrel, barrel/endcap, and endcap/endcap regions. Future analysis could potentially improve significance by applying separate cuts to each region. N_{step}, the number of crystals in the ϕ direction to search to make a barrel supercluster, was also opened for a slight improvement.

3.7 Testing Preshower Calibration

The energy of endcap SuperClusters is corrected for the energy deposited in the preshower $E_{\rm presh}$. This energy is estimated from a calibration procedure using known energy in the strips (and preshower clusters formed from them in X and Y planes) by [**?**]

$$E_{\rm presh} = \gamma(\alpha E_x + \beta E_y) \tag{3}$$

In the current energy correction procedure [1)] we use $\alpha = 0.7$, $\beta = 1.0$ and $\gamma = 0.024$. The latter parameter, γ is a slope for a dependence of energy lost in the preshower on the total energy deposited in the associated preshower clusters (usually expressed in the number of Mips).

To check this dependence, we used single electrons simulated in CMSSW 310_pre6 with flat energy and flat pseudorapidity distributions. We considered just electrons with $1.65 < |\eta| < 2.60$, where we have the preshower

[1)] PreshoweClusterProducer class

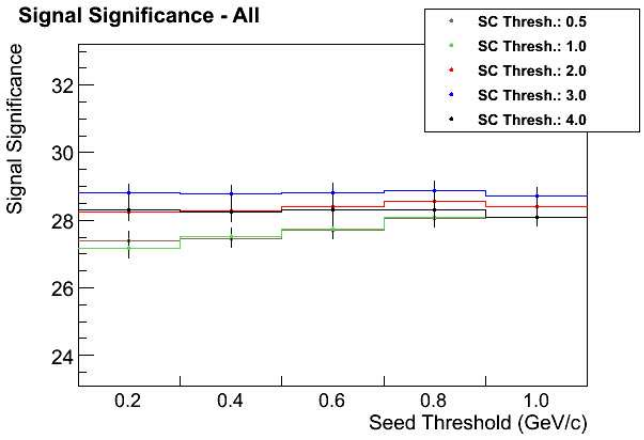

(a) Default ϕ window, with HLT

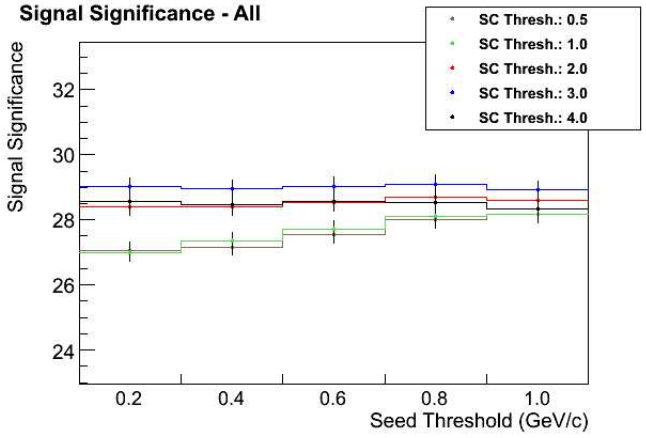

(b) Loose ϕ window, with HLT

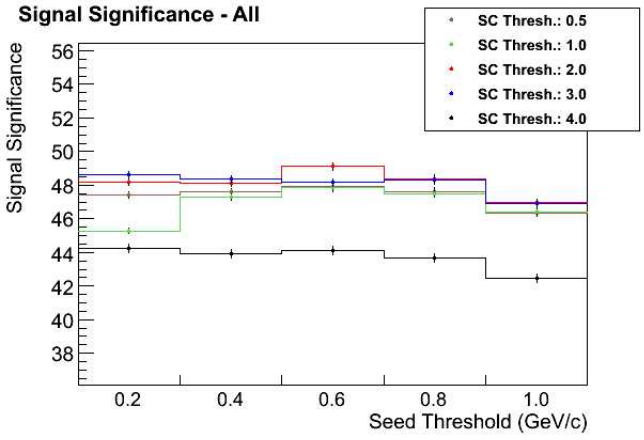

(c) Default ϕ window, no HLT

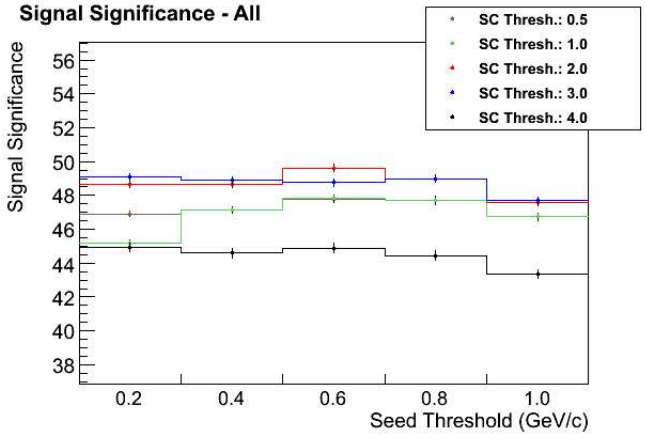

(d) Loose ϕ window, no HLT

Figure 11: Significance tuning for minimum seed E_T and minimum total supercluster E_T. The ϕ window refers to the track seed to supercluster matching and the HLT used is double 3 GeV electron.

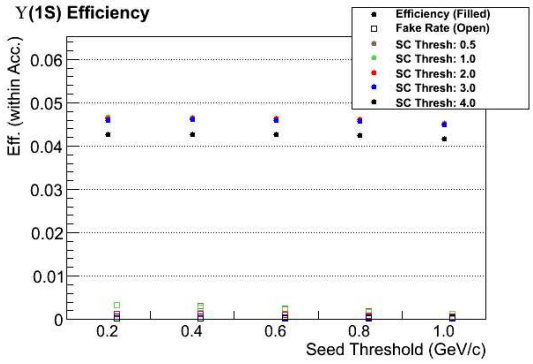

(a) Default ϕ window, with HLT

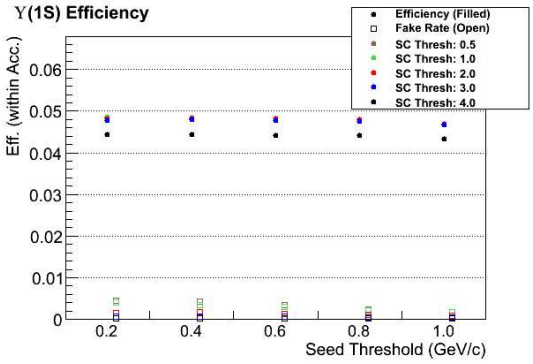

(b) Loose ϕ window, with HLT

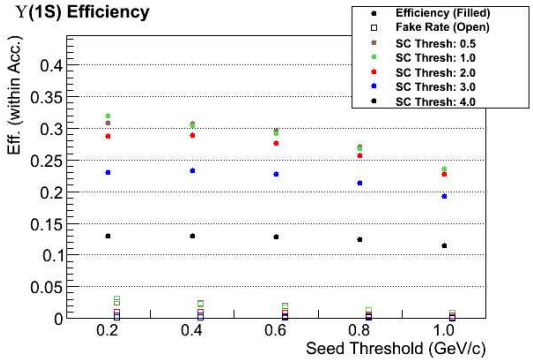

(c) Default ϕ window, no HLT

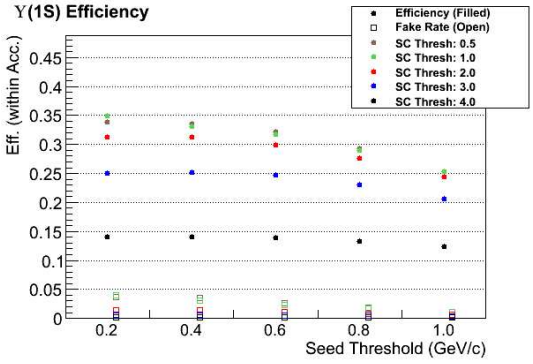

(d) Loose ϕ window, no HLT

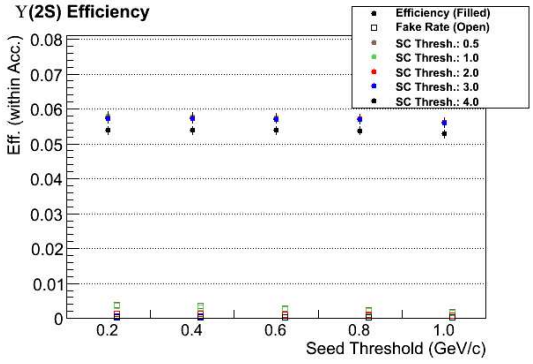

(e) Default ϕ window, with HLT

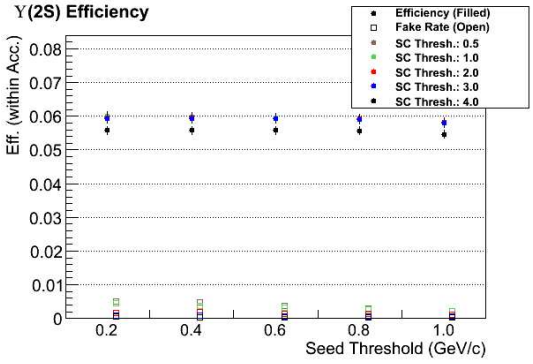

(f) Loose ϕ window, with HLT

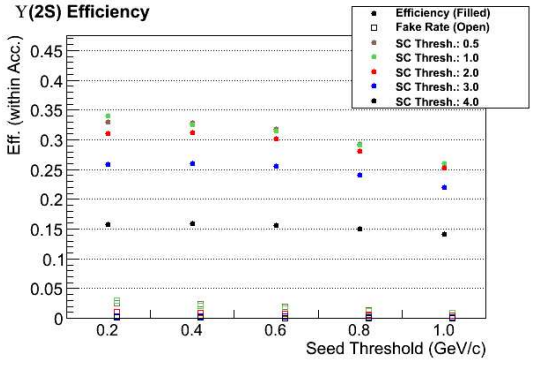

(g) Default ϕ window, no HLT

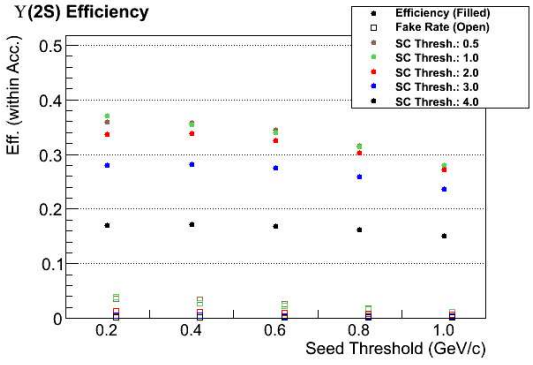

(h) Loose ϕ window, no HLT

Figure 12: Efficiency tuning for minimum seed E_T and minimum total supercluster E_T for Υ(1S)and Υ(2S). The

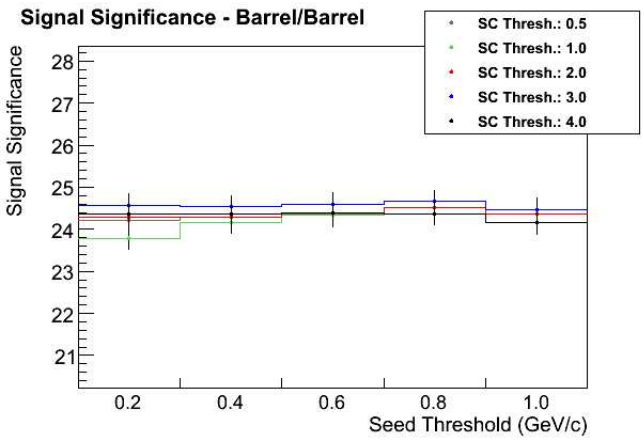

(a) Default ϕ window, with HLT

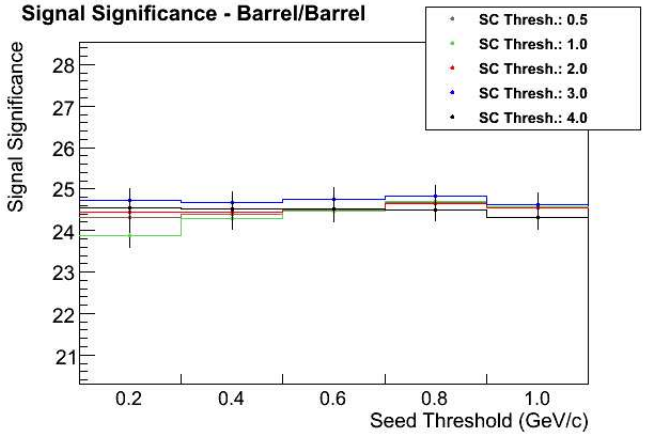

(b) Loose ϕ window, with HLT

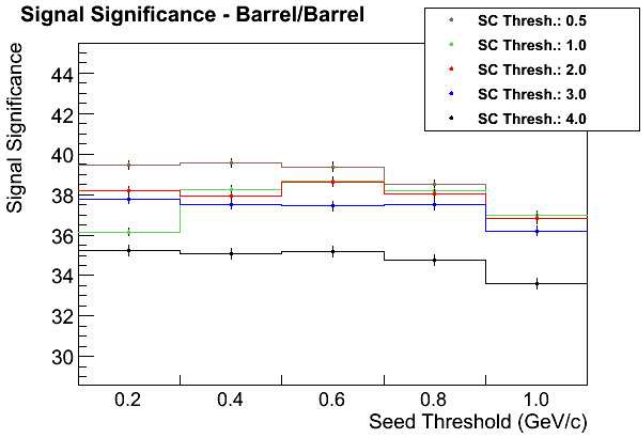

(c) Default ϕ window, no HLT

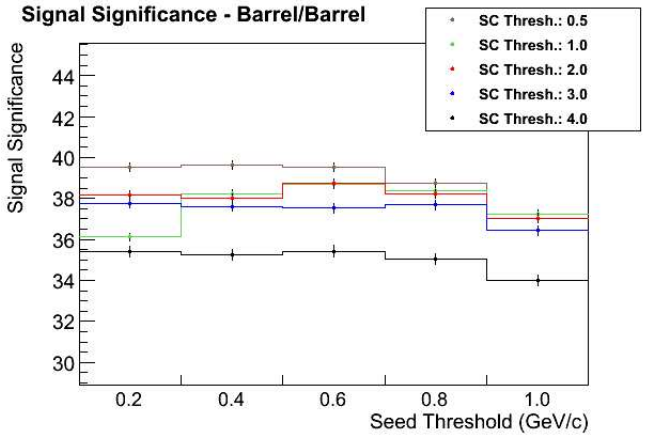

(d) Loose ϕ window, no HLT

Figure 13: Significance tuning for minimum seed E_T and minimum total supercluster E_T for Υ candidates whose daughters are both in the barrel region. The ϕ window refers to the track seed to supercluster matching and the HLT used is double 3 GeV electron.

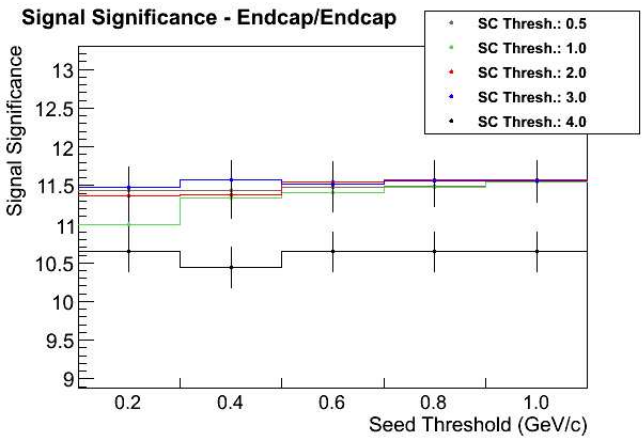

(a) Default ϕ window, with HLT

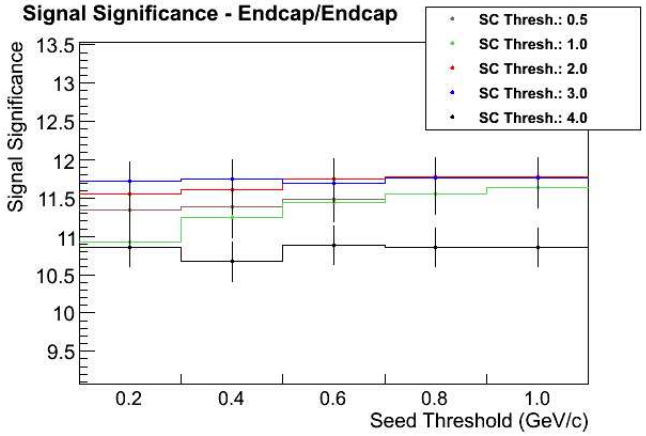

(b) Loose ϕ window, with HLT

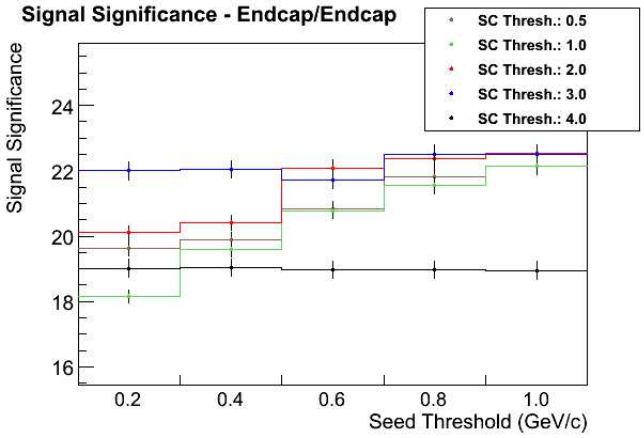

(c) Default ϕ window, no HLT

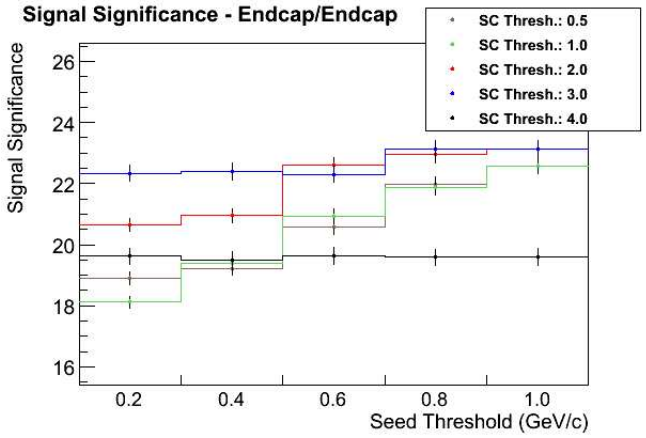

(d) Loose ϕ window, no HLT

Figure 14: Significance tuning for minimum seed E_T and minimum total supercluster E_T for Υ candidates whose daughters are both in the endcap region. The ϕ window refers to the track seed to supercluster matching and the HLT used is double 3 GeV electron.

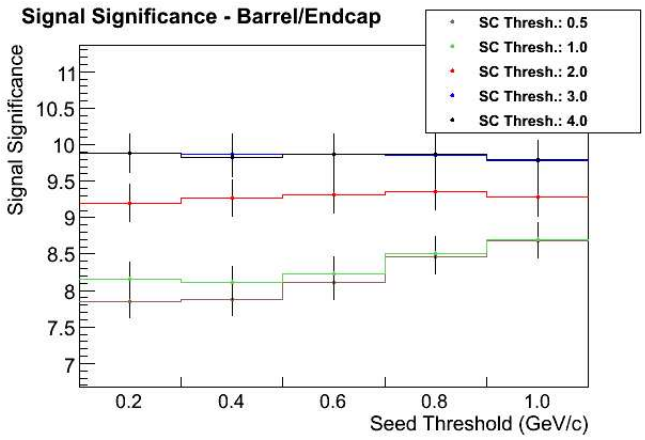

(a) Default ϕ window, with HLT

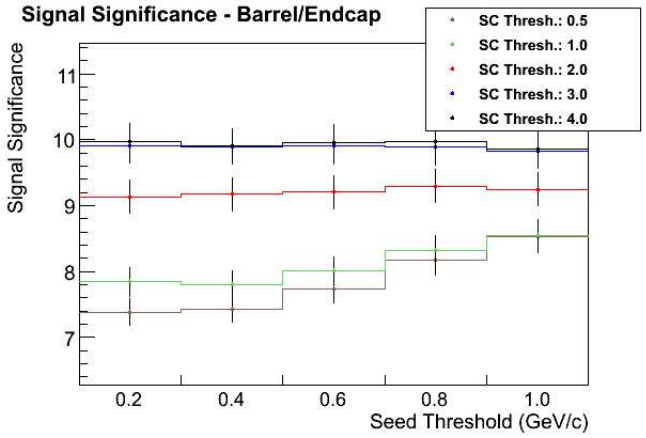

(b) Loose ϕ window, with HLT

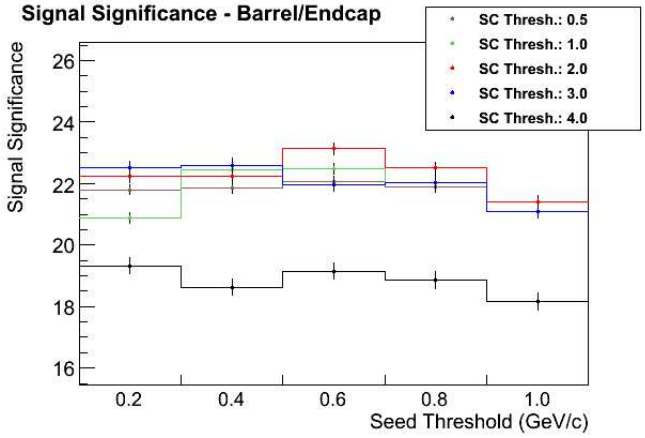

(c) Default ϕ window, no HLT

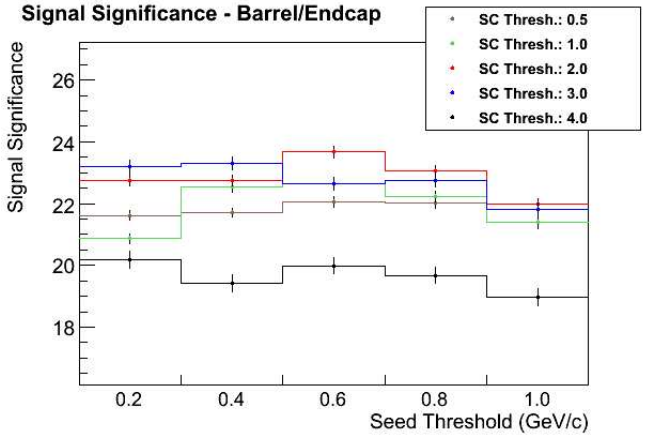

(d) Loose ϕ window, no HLT

Figure 15: Significance tuning for minimum seed E_T and minimum total supercluster E_T for Υ candidates with one daughter in the barrel region and one in the endcap. The ϕ window refers to the track seed to supercluster matching and the HLT used is double 3 GeV electron.

coverage, and $4 < p_T < 10$ GeV. Fig. 3.7 shows dependence of $E_{part} - E_{SC}^{raw}$ versus #Mips in the four electron η intervals. Here E_{part} and E_{SC}^{raw} are true particle level and raw SuperCluster energies and #Mips is the total preshower cluster energy expressed in the number of Mips [2)] We may see quite a good linear dependence between the two quantities which was fitted by a straight line. One can see that the fitted (best) slope is still about within default value of $\gamma = 0.024$ while smaller η's suggest a smaller γ value. To test significance of the found best γ values, we looked at the RMS of distribution for $E_{part} - E_{SC}^{raw}$ versus different γ values. This dependence is shown at Fig. 16. From this figure we may conclude that for high η regions the γ around default value is still preferable choice. The small η's, $1.65 < |\eta| < 1.85$, while prefer a smaller $gamma$, do not exhibit a significant difference with respect to the default one.

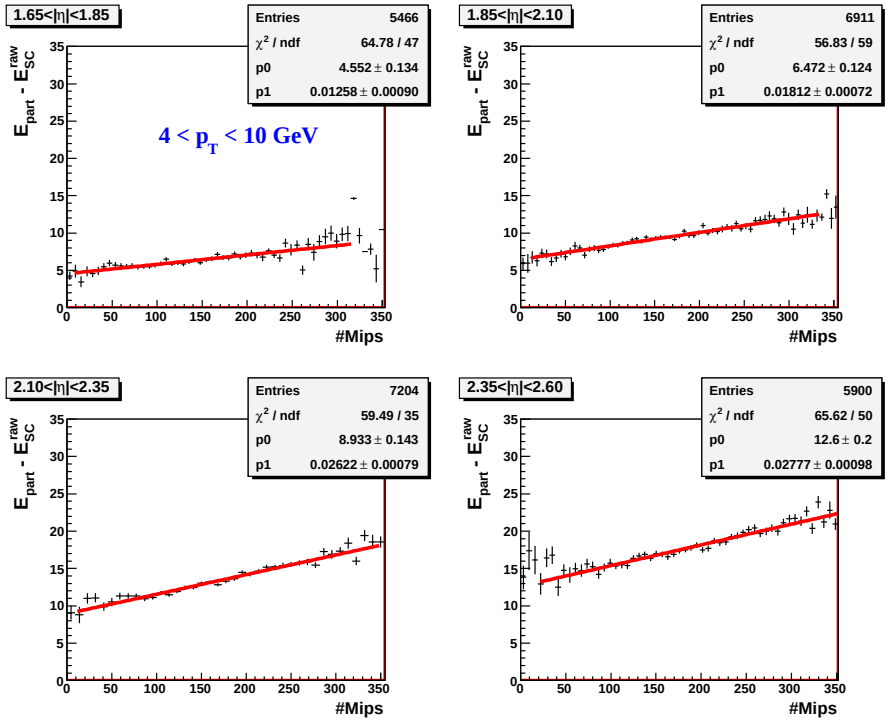

Figure 16: Dependence of energy lost in the preshower on the observable preshower clusters energy, expressed in #Mips.

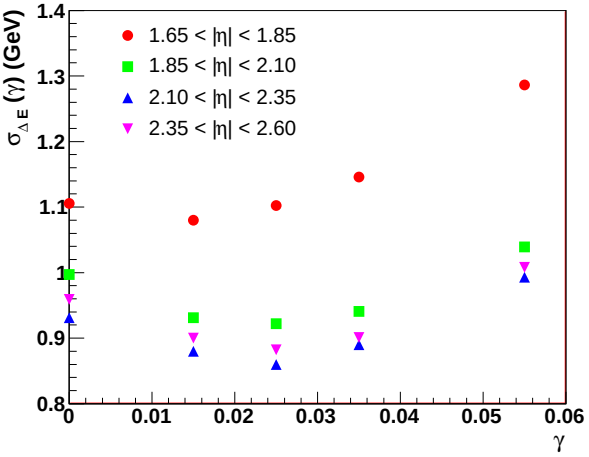

Figure 17: Dependence of $\sigma(E_{part} - E_{SC}^{raw})$ on γ (see the text) for four electron η regions and $4 < p_T < 10$ GeV.

[2)] Here we used value of Mip = 81.08 KeV [**?**].

4 Performance

In this section we compare the results of the re-tuned electron reconstruction algorithms with default[3)] electron reconstruction. The "default" electron reconstruction can be considered in the CMSSW_2_2_X releases, on which the rest of this work is based, and also for the CMSSW_3_1_X releases. In the CMSSW_3_1_X releases the default reconstruction has been updated. In addition for these releases, a "particle flow" electron collection is also available. We consider all three default electron collections.

To compare the results of our re-tuned electron reconstruction with these standard electron reconstruction algorithms, we look at signal $\Upsilon(1S)$ data samples. We start by looking at the performance of the various algorithms in the reconstruction of the electron daughters from the $\Upsilon(1S)$. Figures 18(a) and 18(b) show the electron efficiency from each of the algorithms against the electron p_T and η. The algorithms presented in this note, and re-tuned for low p_T, are the most efficient, gaining noticeably for electrons below 7 GeV/c. In addition the island algorithm is up to 10% more efficient than the same electrons with the hybrid algorithm in the barrel for electron between 2 and 3 GeV/c.

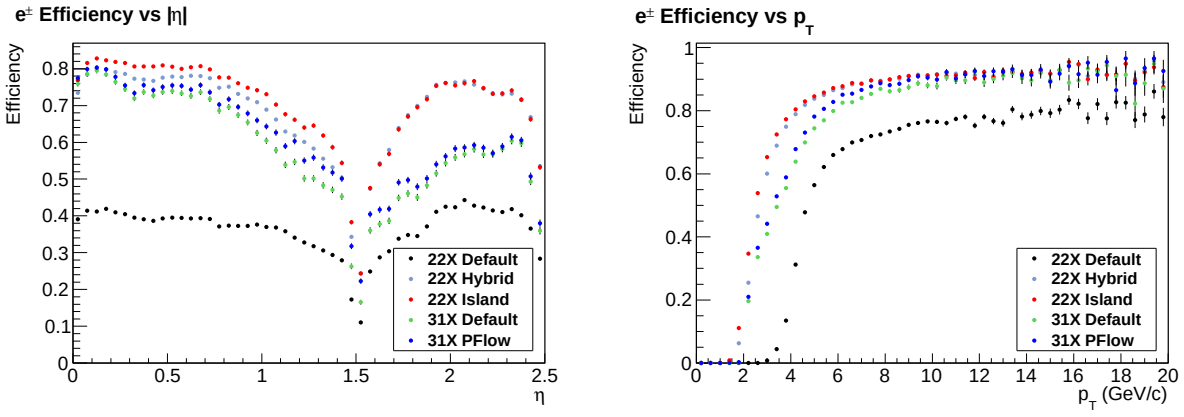

(a) (b)

Figure 18: Electron efficiency of various reconstruction algorithms for electrons from the process $\Upsilon(1S) \rightarrow e^+e^-$. Figure 18(a) show efficiency versus electron η and Figure 18(b) shows efficiency versus electron p_T. The algorithms are labeled as follows: "22X Default" - default electron reconstruction in 22X releases of the CMSSW software, "22X Hybrid" - electron reconstruction re-tuned for low p_T , using hybrid barrel superclusters, "22X Island" - electron reconstruction re-tuned for low p_T , using island barrel superclusters, "31X Default" - default electron reconstruction in 31X releases of the CMSSW software, and "31X PFlow" - particle flow electrons from 31X releases.

Gains in efficiency, however, are no use if they cause the resolution to become unmanageably large. Electron resolution can be evaluated in two ways: by looking at the difference of the measured and true electron p_T's, Δp_T, or by looking at the ratio of the measured p_T to the true p_T, $p_{T,meas}/p_{T,true}$. The two quantities give different information about the reconstruction performance. For each reconstruction algorithm, Figures 19(a) and 19(a) show Δp_T as a function of the true electron η and p_T respectively. Figures 20(a) and 20(a) show $p_{T,meas}/p_{T,true}$ as a function of the true electron η and p_T respectively. The overall distributions for the two resolution variables are also shown in Figure 21. Once again the re-tuned algorithms presented in this note perform better than, or as well as any of the default algorithms.

[3)] Here "default" means any CMS electron reconstruction algorithms that have not been modified in any way

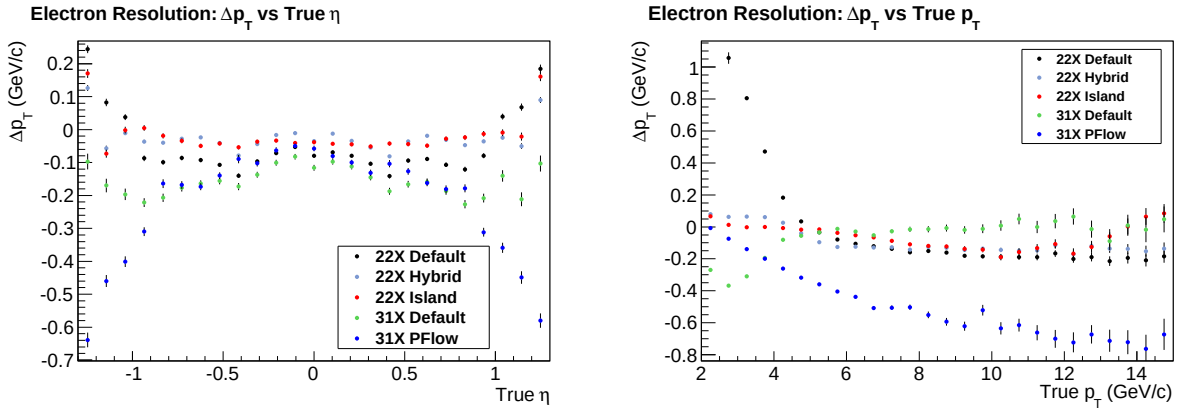

(a) (b)

Figure 19: Electron resolution, Δp_{T}, of various reconstruction algorithms for electrons from the process $\Upsilon(1S) \rightarrow e^{+}e^{-}$. Figure 19(a) shows mean Δp_{T} versus electron η and Figure 19(b) shows mean Δp_{T} versus electron p_{T}. The algorithms are labeled as follows: "22X Default" - default electron reconstruction in 22X releases of the CMSSW software, "22X Hybrid" - electron reconstruction re-tuned for low p_{T} , using hybrid barrel superclusters, "22X Island" - electron reconstruction re-tuned for low p_{T} , using island barrel superclusters, "31X Default" - default electron reconstruction in 31X releases of the CMSSW software, and "31X PFlow" - particle flow electrons from 31X releases.

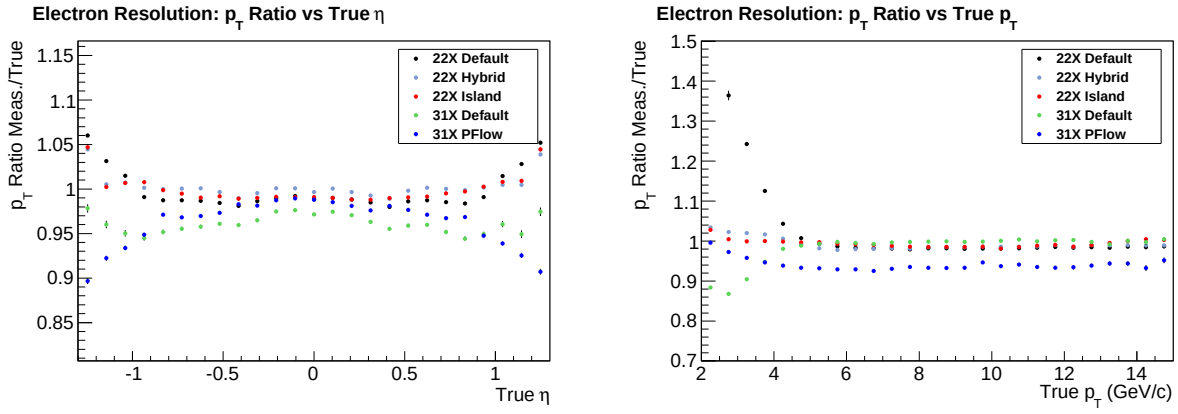

(a) (b)

Figure 20: Electron resolution, $p_{\mathrm{T,meas}}/p_{\mathrm{T,true}}$, of various reconstruction algorithms for electrons from the process $\Upsilon(1S) \rightarrow e^{+}e^{-}$. Figure 20(a) shows mean $p_{\mathrm{T,meas}}/p_{\mathrm{T,true}}$ versus electron η and Figure 20(b) shows mean $p_{\mathrm{T,meas}}/p_{\mathrm{T,true}}$ versus electron p_{T}. The algorithms are labeled as follows: "22X Default" - default electron reconstruction in 22X releases of the CMSSW software, "22X Hybrid" - electron reconstruction re-tuned for low p_{T} , using hybrid barrel superclusters, "22X Island" - electron reconstruction re-tuned for low p_{T} , using island barrel superclusters, "31X Default" - default electron reconstruction in 31X releases of the CMSSW software, and "31X PFlow" - particle flow electrons from 31X releases.

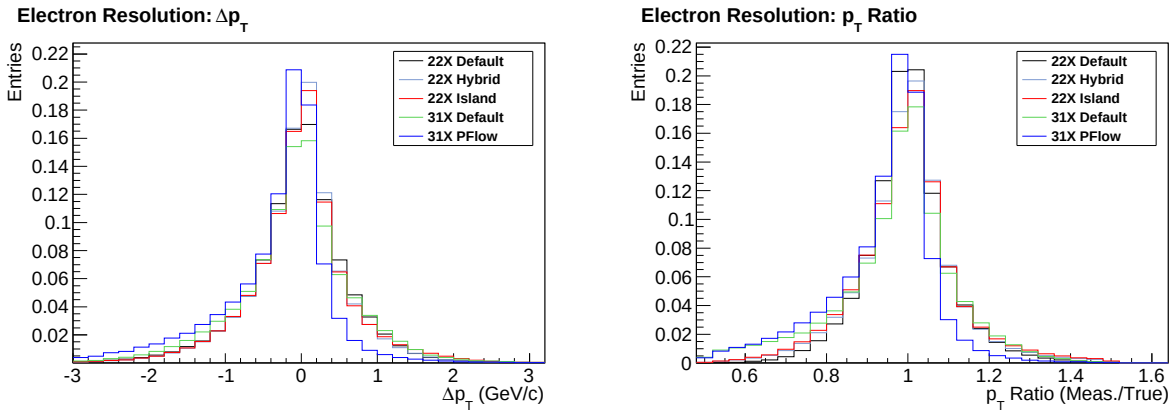

(a) (b)

Figure 21: Electron resolution of various reconstruction algorithms for electrons from the process $\Upsilon(1S) \rightarrow e^+e^-$. Figure 21(a) shows $\Delta p_{\rm T}$ and Figure 21(b) shows $p_{\rm T,meas}/p_{\rm T,true}$. All histograms are normalized to unit area to show the relative shapes. The algorithms are labeled as follows: "22X Default" - default electron reconstruction in 22X releases of the CMSSW software, "22X Hybrid" - electron reconstruction re-tuned for low $p_{\rm T}$, using hybrid barrel superclusters, "22X Island" - electron reconstruction re-tuned for low $p_{\rm T}$, using island barrel superclusters, "31X Default" - default electron reconstruction in 31X releases of the CMSSW software, and "31X PFlow" - particle flow electrons from 31X releases.

The performance of the different reconstruction methods can also be evaluated in terms of the $\Upsilon(1{\rm S})$ efficiency. Figures 22(a) and 22(b) show the $\Upsilon(1{\rm S})$ efficiency from each of the algorithms against the $\Upsilon(1{\rm S})$ $p_{\rm T}$ and η. For the $\Upsilon(1{\rm S})$ it is also important to see the final invariant mass distributions. These are shown in Figure 23. In agreement with the electron performance plots the best $\Upsilon(1{\rm S})$ reconstruction efficiency is achieved with the re-tuned reconstruction algorithms. These algorithms also achieve the best resolution ($\sim$ 500 MeV/c^2). The expense, however, is a slightly higher fake rate (dotted lines in Figure 23). As the significance tuning (see Sec. 3.6) shows, however, this is more than made up for by the gain in signal efficiency.

5 Conclusions

We examined the existing electron reconstruction. The default GSF electron with Hybrid clustering in the Barrel and Multi5x5 in the Endcap, Particle Flow electron. In addition, we reevaluated the GSF electron with Island clustering for electrons with Pt less than 10 GeV. We re-tuned the algorithms for reconstructing the low $p_{\rm T}$ electrons associated with low mass resonance production and found that the re-tuned low $p_{\rm T}$ algorithm using Island superclusters in the barrel and Multi5x5 superclusters in the endcap yield the best efficiency and resolution for $\Upsilon({\rm nS})$ reconstruction. At the time of the write up we did not completed the energy scale correction for Endcap electrons using preshower. An update will be added to note in the very near future.

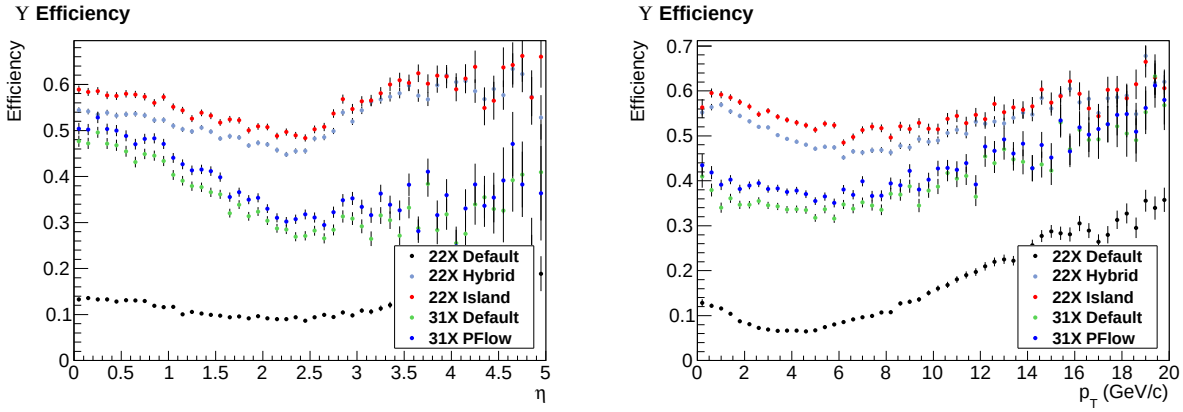

(a) (b)

Figure 22: $\Upsilon(1S)$ efficiency of various reconstruction resulting from the various electron reconstruction algorithms for the process $\Upsilon(1S) \rightarrow e^+e^-$. Figure 22(a) show efficiency versus electron η and Figure 22(b) shows efficiency versus electron p_T. The algorithms are labeled as follows: "22X Default" - default electron reconstruction in 22X releases of the CMSSW software, "22X Hybrid" - electron reconstruction re-tuned for low p_T , using hybrid barrel superclusters, "22X Island" - electron reconstruction re-tuned for low p_T , using island barrel superclusters, "31X Default" - default electron reconstruction in 31X releases of the CMSSW software, and "31X PFlow" - particle flow electrons from 31X releases.

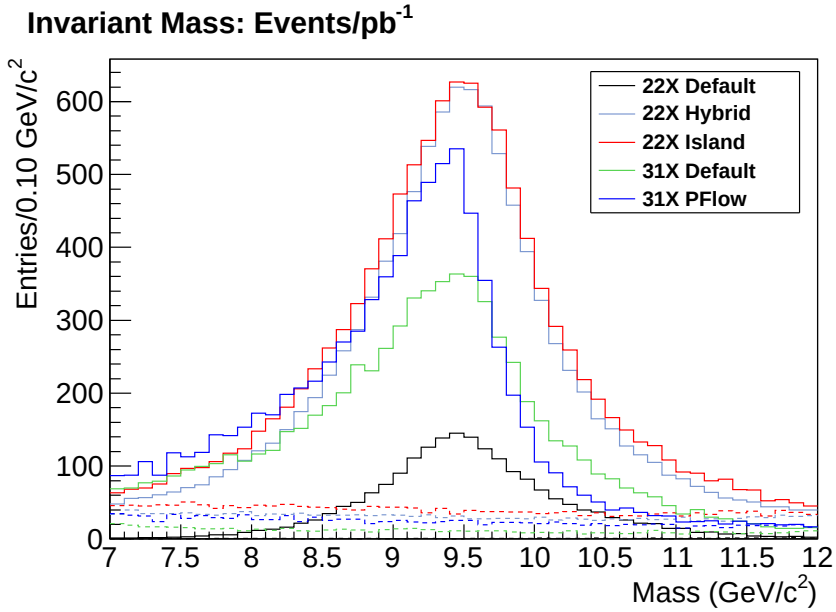

Figure 23: Invariant di-electron mass distributions for $\Upsilon(1S)$ signal MC using the various electron reconstruction algorithms. Solid lines show total distributions, dashed lines give the contribution from fakes. The algorithms are labeled as follows: "22X Default" - default electron reconstruction in 22X releases of the CMSSW software, "22X Hybrid" - electron reconstruction re-tuned for low p_T , using hybrid barrel superclusters, "22X Island" - electron reconstruction re-tuned for low p_T , using island barrel superclusters, "31X Default" - default electron reconstruction in 31X releases of the CMSSW software, and "31X PFlow" - particle flow electrons from 31X releases.

References

[1] C. Amsler et al. The review of particle physics. *Physics Letters B*, 667, 2008.

[2] D. Newbold et al. Electron id at high energies. *CMS AN 2008/045*.

[3] E. Meschi et al. Electron reconstruction in the cms electromagnetic calorimeter. *CMS NOTE 2001/034*.

[4] M. Kraemer. Quarkonium production at high-energy colliders. *arXiv.hep-ph/0106120v1*, 2001.

[5] N. Adam et al. Up coming trigger note. *CMS NOTE 2009/XXX*.

[6] P. Artoisenet et al. υ production at fermilab tevatron and lhc energies. *Physical Review Letters*, 101, 2008.

[7] S. Baffoni et al. Electron reconstruction in cms. *CMS NOTE 2006/040*.

[8] The CMS Collaboration. Cms physics, technical design report, volume: 1 detector performance and software. *CERN/LHCC 2006/001*.

[9] The D0 collaboration. Measurement of the polarization of the $\upsilon(1s)$ and $\upsilon(2s)$ states in $p\bar{p}$ collisions at $\sqrt{s} = 1.96$ tev. *arXiv:0804.2799v2 [hep-ex]*, 2008.

[10] W. Adam et al. Reconstruction of electrons with the gaussian-sum filter in the cms tracker at the lhc. *CMS NOTE 2005/001*.

[11] W. Adam et al. Saturation and energy corrections for tev electrons and photons. *CMS NOTE 2006/149*.